

Pre-stimulus gamma power in human posteromedial cortex shows supra-modal mechanisms in predicting the amplitude and latency of task-induced suppression

Jie Ma^{1,2,†}, Lu Shen^{1,2,†}, Li Song^{1,2}, Qiang Guo³, Josef Parvizi⁴, Biao Han^{1,2,*}, Qi Chen^{1,2,*}

¹Center for Studies of Psychological Application, South China Normal University, Guangzhou 510631, China,

²School of Psychology, South China Normal University, Guangzhou 510631, China,

³Epilepsy Center, Guangdong Sanjiu Brain Hospital, Guangzhou 510510, China,

⁴Department of Neurology and Neurological Sciences, Stanford University, Stanford, CA 94305, USA

*Corresponding authors: Center for Studies of Psychological Application, South China Normal University, Guangzhou 510631, China.

E-mail: biao.han@m.scnu.edu.cn (Biao Han); E-mail: qi.chen27@gmail.com (Qi Chen)

†Jie Ma and Lu Shen contributed equally to the present work.

Upon repetitively performing the same well-practiced task on identical bottom-up stimuli, our performance still varies. Although it has been well documented that elevated pre-stimulus baseline activity in the human default-mode network impairs the subsequent task performance, it remains unknown (i) the fine-grained temporal dynamics and (ii) whether the underlying neural dynamics are supra-modal or modality-specific. We utilized intracranial recordings in the human posteromedial cortex (PMC) during a simple visual and an auditory detection task. Our findings suggested that the pre-stimulus gamma power in PMC predicted the subsequent task performance. Critically, the higher the pre-stimulus gamma power, the longer it took for it to be suppressed, and the less suppressed it was during the task performance, which eventually resulted in deleterious effects on task performance, i.e. longer reaction times. These fine-grained temporal dynamics were consistent between the visual and auditory simple detection task. In addition, a direct comparison between the visual and auditory modality showed that the between-modality difference emerged during the recovery period from the maximal gamma suppression back to the baseline. Taken together, the present results contribute novel spatio-temporal mechanisms in human PMC on how simple detection performance varies across multiple repetitions, irrespective of the sensory modality involved.

Key words: default mode network; pre-stimulus activity; task performance; modality-general; modality-specific.

Introduction

Our brain does not guarantee stable performance upon repetitively performing the same well-practiced behavioral task on the identical bottom-up inputs. Instead, task performance varies on a moment-to-moment basis, e.g. occasionally delayed responses and behavioral errors. The default mode network (DMN) comprises a distributed set of brain regions with high pre-stimulus baseline activity that is suppressed during engagement of the variety of externally goal-directed tasks (Raichle et al. 2001; Raichle and Gusnard 2005; Lachaux et al. 2008; Hayden et al. 2009; Miller et al. 2009; Jerbi et al. 2010; Jung et al. 2010; Dastjerdi et al. 2011; Ossandón et al. 2011; Foster et al. 2012; Fox et al. 2018). Importantly, both the magnitude and the duration of the task-induced DMN suppression correlate with task complexity and performance: the more complex the externally directed tasks, the slower the reaction times (RTs), and the longer and the deeper DMN suppression (Shulman et al. 1997; McKiernan et al. 2003; Ossandón et al. 2011; Foster et al. 2012). Therefore, the task-induced DMN deactivation does not simply represent the relative silencing of a task-irrelevant network, but instead might be an active process of functional suppression important for successful task performance (Fox et al. 2018). On the other hand, the pre-stimulus baseline activity is frequently referred to as background activity because it is not related to the sensory or motor aspects of the task. Thus, it is often subtracted from the measured neural

signals during the task, on the assumption that it represents neural activity noise. However, elevated DMN baseline activity, prior to the actual onset of the behavioral targets, predicts poor task performance, such as occasional lapses in attention (Weissman et al. 2006; Hayden et al. 2009; Kucyi et al. 2020), and failures in perceiving near-threshold somatosensory stimuli (Boly et al. 2007). Therefore, rather than merely reflecting the noise in the system, the baseline signal reflects the cortical manifestation of vigilance state, motivational, or arousal pathways, which determine the efficiency of cortical sensorimotor processing and the quality of the task performance (Zhang et al. 2014).

Although both increased pre-stimulus activity and alleviated task-induced suppression in the DMN have been associated with deteriorating task performance (Weissman et al. 2006; Ossandón et al. 2011; Kucyi et al. 2020), it remains completely unknown how variation in pre-stimulus baseline activity translates to the varying extent of the subsequent task-induced suppression, along both the temporal and the amplitude dimension, which eventually alters behavior. Taking advantage of the high temporal resolution of intracranial electroencephalography (iEEG) in patients with drug-resistant epilepsy and a relatively adequate electrode coverage in the human posteromedial cortex (PMC), a core hub of the DMN, we aimed to investigate the moment-to-moment variation in neuronal activity from the pre-stimulus to the post-stimulus period, which correlates with the varying behavioral performance

Received: September 21, 2022. Revised: February 15, 2023. Accepted: February 16, 2023

© The Author(s) 2023. Published by Oxford University Press. All rights reserved. For permissions, please e-mail: journals.permissions@oup.com

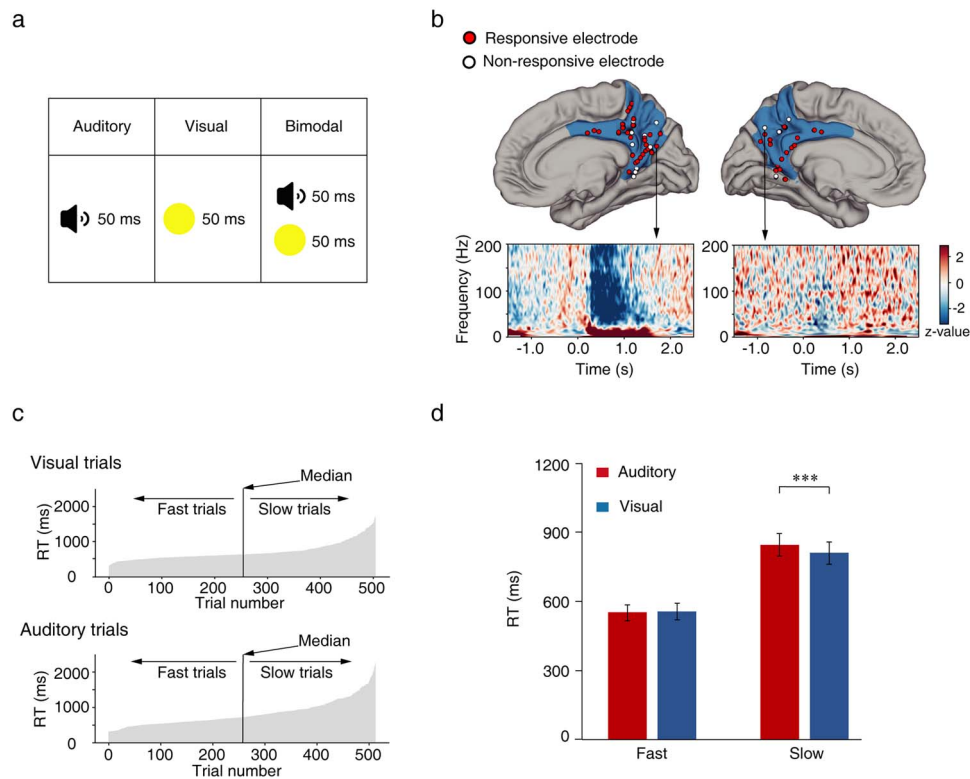


Fig 1. Stimuli, localization of PMC electrode sites, and behavioral performance. (a) There were three types of targets: the unimodal auditory target, the unimodal visual target, or the bimodal audiovisual targets. In each trial, the target was presented for 50 ms, and the subjects were instructed to press one response button if they heard the auditory target, press the other response button if they saw the visual target, and press both buttons if they both saw and heard. And the interval was 2500–2900 ms. Only the two types of unimodal trials were analyzed in the present study. (b) Anatomical and functional locations of the PMC electrodes. The upper panels: all the cortical electrodes falling in the anatomically defined PMC area (shaded in blue) in the 19 participants were projected onto the fsaverage standard space. The red circles represent the functionally responsive electrodes that showed a significant decrease in the gamma power after the target onset, compared with the pre-stimulus baseline, and the white circles represent the non-responsive electrodes. The bottom panels: the time-frequency diagrams show the typical electrophysiological activations in one representative responsive and non-responsive electrode, respectively. (c) Within each type of unimodal trials, the trials were classed into the fast vs. slow trials based on the median of the RTs. (d) Mean RTs of the unimodal visual vs. auditory trials are shown as a function of the fast vs. slow conditions. The error bars indicate the standard error of the mean. *** $P < 0.001$.

upon performing the same behavioral task on identical bottom-up inputs. According to previous evidence (Weissman et al. 2006; Hayden et al. 2009; Kamp et al. 2018; Kucyi et al. 2020), we hypothesized that the magnitude of pre-stimulus baseline gamma band power in the PMC electrodes should predict the subsequent task performance. More critically, we aimed to investigate how the pre-stimulus baseline gamma power determines the quality of task-induced suppression in PMC, in terms of both the magnitude and the latency. We predicted that elevated pre-stimulus baseline gamma power in PMC will result in delayed and alleviated task-induced suppression, and accordingly slower RTs.

In addition, due to differential neuronal properties in the visual vs. auditory pathway (Marshall and Talbot 1942; Kemp Jr et al. 1973; King 2005a), even simple RTs in detection tasks differ between the visual and the auditory stimuli (Dunlap and Wells 1910; Jose and Gideon Praveen 2010). Although the DMN is generally deactivated both during the visual and auditory tasks (Daselaar et al. 2010; Huijbers et al. 2011; Humphreys et al. 2015), it remains unclear (i) whether the fine-grained temporal dynamics of task-induced neural deactivations in the DMN are modality-independent or -specific, and (ii) how the potential between-modality differences vary when the task performance is matched vs. unmatched between the visual and auditory modality. To further answer these questions, we adopted a simple visual or auditory detection task (Fig. 1a). The participants were instructed

to simply detect the appearance of a supra-threshold target delivered either in the auditory or the visual modality.

Materials and methods

Ethics and participants

The data were collected from 19 patients (mean age \pm SD, 23.78 ± 3.41 years; 13 male and 6 female) with drug-resistant focal epilepsy undergoing neurosurgical treatment. The patients were implanted with depth electrodes which were placed within one or both hemispheres. The electrodes were not implanted for the purposes of this study, but only as part of a pre-surgical evaluation to help localize the seizure onset zone. After implantation, the patients were monitored for about two weeks in their hospital rooms. During this period of time, we administered the cognitive task. All the subjects provided written informed consent to participate in the study, and the Ethics Committee of South China Normal University approved all the procedures.

Stimuli and experimental design

There were two types of target stimulus in the experiment: a 4000-Hz pure tone as the auditory target; and a yellow circular stimulus of 1.5° visual angle at the center of the screen as the visual target. The default visual display was a white central fixation cross that measured $1^\circ \times 1^\circ$ of visual angle on a black background. The

Table 1. Demographics and electrode distribution in each patient.

ID	Sex	Age	L/R handed	Epilepsy duration	Ictal or inter-ictal	Task blocks	PMC responsive sites
1	Female	21	R	9 years	Bilateral hippocampus	30	3
2	Male	31	L	—	Left lateral sulcus	62	4
3	Female	23	R	11 years	Left insula and temporal lobe	64	9
4	Male	22	R	2 years	Right intraparietal sulcus and middle temporal area	73	13
5	Male	24	R	18 years	Right cuneus and lingual gyrus	35	3
6	Male	18	R	14 years	Right temporal lobe	15	5
7	Male	23	R	15 years	Left insula and temporal lobe	18	4
8	Male	28	R	20 years	Left intraparietal sulcus and temporal lobe	76	4
9	Male	23	Bi	12 years	Left superior temporal lobe	76	5
10	Male	21	R	1 years	Right orbitofrontal region	64	2
11	Female	22	R	5 years	Left insular and supramarginal gyrus	72	3
12	Male	26	R	6 years	Right orbitofrontal region and temporal pole	64	3
13	Male	27	R	23 years	Right insula and temporal lobe	17	5
14	Male	27	R	—	Bilateral parieto-occipital regions	30	12
15	Female	29	R	21 years	Left medial temporal lobe	15	2
16	Male	21	Bi	5 years	Left medial temporal lobe	32	1
17	Female	26	R	12 years	Right medial temporal lobe	18	5
18	Female	20	R	5 years	Right inferior temporal lobe	18	2
19	Male	20	R	11 years	Right central sulcus	18	4

L: left, R: right, Bi: bilateral, —: information missing.

inter-trial interval (ITI) was randomized from 2500 to 2900 ms (i.e. 2500, 2600, 2700, 2800, and 2900 ms). There were three types of trials: (i) the unimodal auditory trials, in which the auditory target was presented for 50 ms; (ii) the unimodal visual trials, in which the visual target was presented for 50 ms; and (iii) the bimodal audiovisual trials, in which the visual and auditory targets were simultaneously presented for 50 ms (Fig. 1a). Participants were instructed to press one response button if they saw the visual target, press the other response button if they heard the auditory target, and press both buttons if they both saw and heard. The mapping between the auditory and the visual targets and the two response keys was counterbalanced within each subject. The experiment was scripted and run by Presentation software (Neurobehavioral Systems, RRID: SCR_002521, <https://www.neurobs.com/>). The auditory target was delivered via loudspeakers placed behind the computer monitor. The visual target was presented on a 23-inch screen (resolution, 1920 × 1080) that positioned ~60 cm from the patients at the eye level.

The experiment was administered in multiple blocks for each patient. The number of blocks obtained from each patient depended on the amount of time available for research recording in the clinical environment, which varied across patients (please see Table 1 for the number of blocks obtained from each patient). There were 50 trials in each block, among which the proportion of visual, auditory, and audiovisual trials was 2:2:1. In the present study, we were only interested in the single modality visual and auditory trials.

Acquisition and preprocessing of the intracranial data

The intracranial EEG (iEEG) recordings were made at the bedside of the subjects' private clinical room. Data were recorded using the clinical monitoring system from Nihon Kohden (Tokyo, Japan) with a sampling rate of 1000 Hz and a band-pass filter of 1–300 Hz. The diameter of each electrode was 0.8 mm, and the inter-electrode spacing was 1.5 mm. The neuroanatomical targets and numbers of electrodes implanted in each subject varied exclusively according to clinical requirements.

Data analysis was performed using Fieldtrip toolbox (RRID: SCR_004849, <http://www.fieldtriptoolbox.org/>, Oostenveld et al. 2011) implemented in MATLAB 2021a (MathWorks, RRID: SCR_001622, <https://www.mathworks.com/products/matlab.html>). For the offline analyses, the recorded signals were first down-sampled to 500 Hz. Subsequently, notch filtering (zero-phase, third order, Butterworth filter with band-stop within 47–53, 97–103, and 147–153 Hz) was performed to remove the power line noise. Each electrode was re-referenced with respect to its direct neighbor, i.e. bipolar montage. As we were interested in both the pre- and the post-stimulus phase, we need to make sure that the pre-stimulus phase of each trial epoch was not contaminated by the manual response of the previous trial, and in the meanwhile keep the pre-stimulus epoch as long as possible. In this study, the ITI between the presentation of the target stimuli in two consecutive trials was jittered from 2500 to 2900 ms in a 100-ms step (i.e. 2500, 2600, 2700, 2800, and 2900 ms), with the minimum ITI being 2500 ms. To achieve a clean pre-stimulus period without contaminations from the response of the previous trial, the RT of the current trial plus the duration of the pre-stimulus epoch should be less than the minimum ITI (i.e. 2500 ms). In the current analyses, we aimed to get a long enough and clean pre-stimulus phase of 1000 ms. Accordingly, the slowest RT of the previous trial has to be “the minimum ITI (2500 ms) - the desired duration of the pre-stimulus epoch (1000 ms)” = 1500 ms. We thus further excluded the correct trials (5%) with RTs longer than 1500 ms from further analyses. Subsequently, the continuous EEG data were segmented into epochs of 3 s, including 1 s before and 2 s after the stimulus onset. After that, the artifact rejection was performed in two steps. First, we applied the methods implemented in the MATLAB-based LBCN preprocessing pipeline (https://github.com/LBCN-Stanford/Preprocessing_pipeline), consistent with previous work (Foster et al. 2012; Kucyi et al. 2020), to reject the bad channels and trials. After that, noisy trials were excluded via visual inspections, which were done blindly irrespective of the experimental conditions.

Time-frequency transformation was performed for each trial using the complex Morlet wavelets with frequencies of interest

between 1 and 200 Hz, in 2-Hz steps. We used wavelet kernels with a variable number of cycles, which linearly increased from 3 to 20 cycles. As we were interested in the pre-stimulus baseline activity, no baseline correction was applied to the data. Instead, we z-transformed (i.e. normalized) the iEEG power data within each frequency and each channel for the auditory and the visual trials, respectively, to address the band-specific $1/f$ drop of the power spectrum (Miller et al. 2007). Specifically speaking, within trials of each modality, the power of each trial was first subtracted by the mean of the grand average of all trials across the epoch time, and then divided by the standard deviation across the epoch time of the grand average of all trials. The z-transformation was applied to all the trials of the same modality, irrespective of the RTs, and thus this normalization does not affect the difference in pre-stimulus gamma power between fast and slow trials. Further data analyses were based on the normalized data, except for the direct comparison between the visual and auditory trials via which we were most interested in the post-stimulus task-induced deactivation. In the latter case, the data analyses were based on the baseline-corrected data: the power spectrum was converted to z-scores using the mean and the standard deviation of the pre-stimulus baseline time window (-1 to -0.1 s).

Localization and visualization of electrodes

Anatomical locations of electrodes were determined via the co-registration between the pre-implantation MRIs and the post-implantation CTs. The registered images were carefully visually checked to ensure adequate registrations. The anatomical locations of electrodes were then labeled by the method implemented in SEEGA (Narizzano et al. 2017) and plotted using 3D slicer (RRID: SCR_005619, <https://www.slicer.org>). To identify the anatomical structure of each electrode, we processed and reconstructed the structural MRI of each subject using Freesurfer v6.0.0 (recon-all command) (RRID: SCR_001847, <https://surfer.nmr.mgh.harvard.edu/fswiki/FreeSurferWiki>, Fischl et al. 2002). The anatomical structures were labeled according to the FreeSurfer Desikan-Killiany atlas (Desikan et al. 2006) using automatic subcortical segmentation and surface parcellation based on gyri and sulci. The PMC area was anatomically defined here as the posterior cingulate cortex, the precuneus cortex, and the isthmus-cingulate cortex. All the electrodes that fall in the above anatomically defined PMC area were first selected.

Furthermore, the electrophysiological signature of the DMN can be effectively represented by the deactivation of gamma power during externally oriented cognitive tasks (Lachaux et al. 2008; Miller et al. 2009; Jerbi et al. 2010; Dastjerdi et al. 2011; Fox et al. 2018). Therefore, we expected to observe a significant task-induced gamma deactivation for the functionally involved PMC electrodes during the performance of the current task. We adopted the Wilcoxon signed-rank test to compare the mean gamma power during the post-stimulus period (0 to 1 s) vs. the pre-stimulus baseline period (-1 to 0 s). Based on this procedure, we functionally selected the PMC electrodes which showed significant task-induced deactivation in gamma power during the post-stimulus period, compared with the pre-stimulus baseline. Only the functionally selected PMC electrodes were entered into further analyses.

To further characterize the anatomically and functionally selected PMC electrodes, a coherence analysis was performed to estimate the degree of signal independence. Specifically, the time series of gamma power during each trial (-1 to 2 s) was first extracted and then joined together for each electrode. A Spearman correlation analysis was then performed on the joined

time series between each pair of electrodes within each subject. The percentage of significantly and positively correlated electrode pairs was used to characterize the signal independence between the selected PMC electrodes.

For visualization purposes, we projected each patient's electrodes to a standard Montreal Neurologic Institute (MNI) reference brain, to get the MNI coordinates of all electrodes. Using iELVis (RRID: SCR_016109, <http://ielvis.pbworks.com>, Groppe et al. 2017), the MNI coordinates of all the anatomically and functionally localized PMC electrodes were projected to fsaverage standard space for visualization purposes (Fig. 1b).

Analysis of behavioral data

For the single modality auditory and visual trials, error trials, including behaviorally missed trials (2%) and incorrect responses (3%), were excluded from further analysis. Additionally, correct trials with RTs longer than 1500 ms (5%) were excluded from further analyses on RTs, to allow for an adequately long pre-stimulus period for the analysis of neural data. Further, among the correct trials, the outlier trials (1%) with RTs outside the range of mean RTs ± 3 SD in each condition were also excluded from further analyses on the RTs. The remaining correct trials (without errors, outliers, and correct trials with RTs longer than 1500 ms) in each modality were then split into the fast and slow conditions according to the median RT in the visual and auditory trials, respectively (Fig. 1c). Mean RTs were then submitted to a 2 (sensory modality: visual vs. auditory) \times 2 (response speed: fast vs. slow) repeated measures ANOVA. Planned paired t-tests (with Bonferroni correction) were used to test the simple effects in case the interaction was significant.

Analysis of neural data

The effect of pre-stimulus power in DMN. To investigate how the pre-stimulus power predicted the subsequent task performance, we performed two steps of analyses. First, by treating the variance of task performance as a dichotomous variable, we directly compared the temporal dynamics of neurophysiological signals between the fast and slow trials. Second, by treating the variance of task performance as a continuous variable, in terms of moment-to-moment variance in RTs, we further correlated the pre-stimulus power in the DMN with the subsequent RTs in each trial (bin). Specifically speaking, within each sensory modality, we first compared the power spectrum of the fast vs. slow trials, using a non-parametric cluster-based permutation test that corrects for multiple comparisons. In this way, we were able to identify the differences in the power spectrum between the fast and the slow trials, both during the pre-stimulus and the post-stimulus periods. To further demonstrate the temporal dynamics of the electrophysiological responses in DMN during the fast vs. slow trials, we averaged the power across the gamma frequencies (30–200 Hz) and the alpha frequencies (8–12 Hz) for the fast and slow trials, respectively. To avoid the problem of double dipping (Kriegeskorte et al. 2009, 2010), no further statistical analysis was performed on the temporal profile of gamma and alpha between the fast and slow trials. Further, we adopted the linear mixed model (LMM) to test the correlation between the pre-stimulus gamma power in the DMN and the trial-by-trial variance in RTs. The pre-stimulus gamma power was calculated as the mean power within the cluster which showed significant differences in the gamma (30–200 Hz) power between the fast and the slow trials during the pre-stimulus period. In the LMM, subjects were entered as a random factor, the pre-stimulus gamma power was

entered as a fixed factor, and the RTs were entered as the dependent variable. To better illustrate the correlation results, for each subject, we first sorted the trials in the ascending order based on the pre-stimulus gamma power, and then grouped every 10 trials into a trial bin along the continuum of the pre-stimulus gamma power. As the number of trials in each subject varied, the resulted number of trial bins varied across subjects (13–140 trial bins). Subsequently, the correlation coefficient between the pre-stimulus gamma power and the RTs was computed for each electrode, based on the merged trial-bin data.

To further investigate how the pre-stimulus gamma power modulated the post-stimulus task-induced deactivation in the gamma power, we calculated the post-stimulus trough gamma power latency and power. We adopted a method on identifying the task-induced maximal gamma suppression in the DMN similar to that employed in prior research (Kucyi et al. 2020). Specifically, the maximal suppression was defined as the lowest gamma power, and the maximal suppression latency was defined as the time interval between the time point of stimulus onset and the maximal gamma suppression, within a time window of 0–2 s after the stimulus onset. We used paired *t*-tests to test whether there was a significant difference between the fast and slow trials, in terms of the maximal suppression latency and the maximal suppression power of the post-stimulus task-induced gamma deactivation. Furthermore, the correlations between the pre-stimulus gamma power and the post-stimulus trough gamma latency and power were calculated via the LMM, respectively. In the LMM, subjects were entered as a random factor, the pre-stimulus gamma power was entered as a fixed factor, and the latency and the power of the maximal gamma suppression were entered as the dependent variable, respectively. Correlation analyses for each electrode were also carried out based on the merged trial-bin data.

Modality-specific mechanisms in the DMN. To further investigate the sensory modality difference in the post-stimulus DMN responses, we directly compared the time course of the gamma power in DMN between the visual and the auditory trials. As the auditory responses were slower than the visual responses in the present study, task difficulty could be a potential confounding factor here. As the auditory responses were slower than the visual responses only in the slow trials, but not in the fast trials, we further compared the visual and auditory processing within the faster and the slow trials, respectively. To further prove the consistency of the results, we categorized the subjects into the response matched and the response unmatched groups, according to the group mean RT difference between the visual and auditory trials across all the subjects. The group mean RT difference was 17 ms, and we rounded it up to 20 ms as a cutoff to categorize the subjects. The subjects, whose absolute RT difference between the visual and auditory trials was less than 20 ms, were categorized as the response matched group (8 subjects), and the rest of the subjects as the response unmatched group (11 subjects).

Statistical analysis

A non-parametric statistical test based on the cluster-level permutation was used to statistically compare the power spectrum and the temporal profile of the gamma power between the fast and slow conditions (Maris and Oostenveld 2007). The cluster-based permutation identifies patterns of oscillatory neural activity and appropriately deals with the multiple comparisons problem. Specifically, every sample between conditions was compared by a paired-samples *t*-test, and the samples were selected if their statistical value was more significant than a threshold ($P = 0.05$,

two-tail) and combined into clusters based on adjacency. The *t*-values within each cluster were summed up as the cluster-level statistics. The random permutation of data was then performed by exchanging the data between conditions across electrodes. The permutation was performed 1000 times (i.e. 1000 random partitions) and the maximum cluster-level statistic was recorded in each permutation run, which resulted in a distribution of the cluster-level test statistic based on the 1000 permutations. The corrected *P*-value was computed by calculating the proportion of random partitions that exceeded the observed (true) test statistic. The clusters in which the summed *t*-values exceeded 95% of the distribution of surrogate clusters (corresponding to a corrected $P < 0.05$) were considered as significant.

We adopted the LMM to calculate the relationship between the pre-stimulus gamma power of the DMN, the subjects' behavioral performance, the post-stimulus trough gamma latency and power in the DMN. The LMM analyses allow to control for data-dependencies within a subject (Baayen et al. 2008). In the current study, the LMMs were computed with the lme4 package (RRID: SCR_015654, <https://cran.r-project.org/web/packages/lme4/index.html>, Baayen et al. 2008; Bates et al. 2015), and the *P*-values were obtained via the lmerTest package (RRID: SCR_015656, <http://CRAN.R-project.org/package=lmerTest>, Kuznetsova et al. 2017) implemented in R. The data were fitted with a random intercept model with the relevant fixed factors and a random factor of subjects. The pre-stimulus gamma power was entered as a fixed factor, the subjects were entered as a random factor, and the predicted variable (i.e. the RTs, or the power or latency of the maximal gamma suppression) was entered as the dependent variable. The coefficients of the LMMs were used to represent the correlation between the predictors and the outcome variables. For each LMM, the significance of the pre-stimulus gamma power in predicting each variable was assessed with the significance level at 0.05.

Results

Behavioral results

The accuracy in the visual (mean \pm SD, $94 \pm 4\%$) and auditory ($96 \pm 4\%$) trials was both around 95%, indicating that the present supra-threshold stimulus detection task was easy enough for both sensory modalities.

The mean RTs were submitted to a 2 (sensory modality: visual vs. auditory) \times 2 (response speed: fast vs. slow) repeated-measures ANOVA. The main effect of sensory modality was significant, $F_{(1,18)} = 4.20$, $P = 0.05$, $\eta^2 = 0.19$, indicating that the mean RTs to the auditory targets (mean \pm SE, 703 ± 40 ms) were slower than to the visual targets (686 ± 42 ms). The main effect of response speed was significant as well, $F_{(1,18)} = 146.04$, $P = 4.51 \times 10^{-10}$, $\eta^2 = 0.89$. Moreover, the interaction between sensory modality and response speed was also significant, $F_{(1,18)} = 16.67$, $P = 0.001$, $\eta^2 = 0.48$. Further planned paired *t*-tests on simple effects showed that the visual (557 ± 33 ms) and auditory (556 ± 30 ms) RTs were comparable for the fast trials, $t_{(18)} = 0.21$, $P = 0.83$, $d = 0.01$, whereas the visual responses (814 ± 52 ms) were significantly faster than the auditory responses (850 ± 52 ms) for the slow trials, $t_{(18)} = -3.12$, $P = 6.42 \times 10^{-3}$, $d = -0.16$ (Fig. 1d).

Please note, the above behavioral results were based on all the correct trials with RTs faster than 1500 ms for the purposes of analyzing the pre-stimulus period of the neural data (see Methods). If we included the correct trials with RTs longer than 1500 ms in the analysis of the behavioral data, consistent patterns were revealed (Supplementary Fig. 1), indicating that removing the correct trials

with RTs longer than 1500 ms did not dramatically alter the behavioral results.

Neural results

A total of 181 electrodes from 19 patients with drug-resistant epilepsy were anatomically localized in the PMC, a core hub of the DMN (see Methods). The PMC electrodes with pathological artifacts were removed via a semi-automatic method (see Methods), leaving 116 PMC electrode sites without visible physiological signal contaminations. Furthermore, the classical electrophysiological profile of the DMN is characterized by the task-induced suppression in the high gamma power (Lachaux et al. 2008; Miller et al. 2009; Jerbi et al. 2010; Dastjerdi et al. 2011; Fox et al. 2018). Therefore, among the 116 anatomically localized and artifacts free PMC electrodes, we further functionally localized 89 electrodes which showed significant task-induced gamma (30–200 Hz) power deactivation during the post-stimulus period (0 to 1 s), compared with the pre-stimulus baseline (–1 to 0 s). As shown in Fig. 1(b), the red circles are the electrodes with the gamma deactivation, and the white circles are the electrodes without the gamma deactivation. The 89 anatomically and functionally localized PMC electrodes were then included in the following analyses. By correlating all electrode pairs in the same subject, we found that the gamma activity of the selected electrodes in the PMC was highly consistent, with 93% of the electrode pairs having a significant positive correlation (see Supplementary Fig. 2).

Pre-stimulus baseline gamma power predicted both magnitude and latency of task-induced deactivation in PMC, irrespective of the sensory modality involved

First, differences in the normalized iEEG power spectrum between the fast and the slow trials were calculated for the visual and the auditory modality, respectively. For the auditory trials, two significant high frequency clusters, covering both the pre-stimulus and the post-stimulus periods, showed significantly lower gamma power in the fast trials than in the slow trials, $P=0.001$, cluster-based permutation (Fig. 2a). In addition, a significant low frequency pre-stimulus cluster, centering at the alpha-band (8–12 Hz), showed significantly higher power in the fast trials than in the slow trials, $P=0.001$, cluster-based permutation (Fig. 2a). The LMM coefficient was calculated to further verify whether there was a significant correlation between the pre-stimulus gamma/alpha power and the RTs. The results showed a significant LMM coefficient of $\beta=2.85$, $P < 2 \times 10^{-16}$, for the pre-stimulus gamma power and the RTs, and a significant LMM coefficient of $\beta=-1.77$, $P=0.04$, for the pre-stimulus alpha power and the RTs. To better illustrate the correlation between the pre-stimulus gamma/alpha power and RTs, we sorted all the trials based on the pre-stimulus gamma power, and grouped every 10 trials into a trial bin along the continuum (see Methods). Correlation coefficient between the pre-stimulus gamma/alpha power and RTs was calculated for each and every electrode, based on the trial-bin data. In sum, 83% of the electrodes showed a positive correlation coefficient between the pre-stimulus gamma power and the RTs (Fig. 2b), and 66% of the electrodes showed a negative correlation coefficient for the pre-stimulus alpha power and the RTs (Fig. 2c). For demonstration purposes, the linear correlation between the pre-stimulus gamma/alpha power and RTs was shown in one representative electrode: the trials with higher pre-stimulus gamma power were associated with slower

RTs (Fig. 2b, the scatter figure), and the trials with higher pre-stimulus alpha power were associated with faster RTs (Fig. 2c, the scatter figure). Taken together, upon detecting supra-threshold auditory targets, the pre-stimulus gamma and alpha power in the DMN predicted the subsequent task performance: the higher the pre-stimulus gamma power, the lower the pre-stimulus alpha power, and the worse the task performance (slower RTs).

To better delineate how the pre-stimulus gamma power affected the task-induced temporal dynamics of gamma, depending on the fast vs. slow trials, the iEEG power spectrum was averaged across the gamma band (30–200 Hz), and displayed as a function of the fast vs. slow trials (Fig. 2d, upper panel). The frequency range was determined based on the significant pre-stimulus time-frequency cluster (fast vs. slow trials) which ranged from 30 to 200 Hz (Fig. 2a). For the gamma power, the time-series data showed that the pre-stimulus baseline activity was already lower in the fast than slow trials. Upon the onset of the targets at time 0, the gamma power started to be deactivated, and the gamma power kept to be lower in the fast than the slow trials during the progress of neural deactivation toward its maxima. After the task-induced gamma deactivation reached its maxima, the gamma power started to recover to the baseline activity, at a faster speed in the fast than slow trials (Fig. 2d, upper panel). To avoid the problem of double dipping (Kriegeskorte et al. 2009, 2010), no statistical tests were performed on the time-series data. In addition, to cross-validate our findings, we conducted the same analyses based on the classically defined high frequency band (HFB, 70–200 Hz). Similar temporal profiles and differences between the fast and slow trials were validated (Supplementary Fig. 3).

To further investigate how the pre-stimulus baseline gamma power in the PMC pre-determined the quality of task-induced gamma deactivation in the PMC, we first compared the fast and slow auditory trials, in terms of the latency and the power of the task-induced maximal gamma deactivation, via planned paired-samples t-tests. For the gamma power, the results suggested that the fast auditory trials showed earlier onset (fast auditory trials: 497 ± 28 ms; slow auditory trials: 678 ± 38 ms, Fig. 2d upper panel, the left inserted bar figure), $t_{(88)} = -4.97$, $P = 8.71 \times 10^{-5}$, $d = -0.58$, and higher magnitude (normalized amplitude in fast auditory trials: -1.90 ± 0.05 , in slow auditory trials: -1.68 ± 0.05 , Fig. 2d, upper panel, the right inserted bar figure), $t_{(88)} = -3.62$, $P = 4.89 \times 10^{-4}$, $d = -0.46$, of task-induced gamma deactivation than the slow auditory trials. To further confirm these results, the LMM were adopted to test the effect of moment-to-moment variance. The results showed that the pre-stimulus gamma power was a significant predictor of both the latency, $\beta=5.73$, $P < 2 \times 10^{-16}$, and the power, $\beta=0.12$, $P < 2 \times 10^{-16}$, of the task-induced maximal gamma deactivation. In contrast, no significant difference in the post-stimulus peak alpha latency, $t_{(88)} = -1.14$, $P=0.26$, $d=-0.14$, and peak alpha power, $t_{(88)} = 0.75$, $P=0.45$, $d=0.12$, was found between the fast and slow auditory trials (Fig. 2d, lower panel).

Furthermore, 84% of the electrodes showed a positive correlation coefficient between the pre-stimulus gamma power and the latency (Fig. 2e), and 82% of the electrodes with the power (Fig. 2f) of the task-induced maximal gamma deactivation. The linear correlation between the pre-stimulus gamma power and the latency (Fig. 2e, the scatter figure) and the power (Fig. 2f, the scatter figure) of the task-induced maximal gamma deactivation was shown in a representative electrode, respectively. The trials with higher pre-stimulus gamma power were associated with later onset and alleviated task-induced gamma

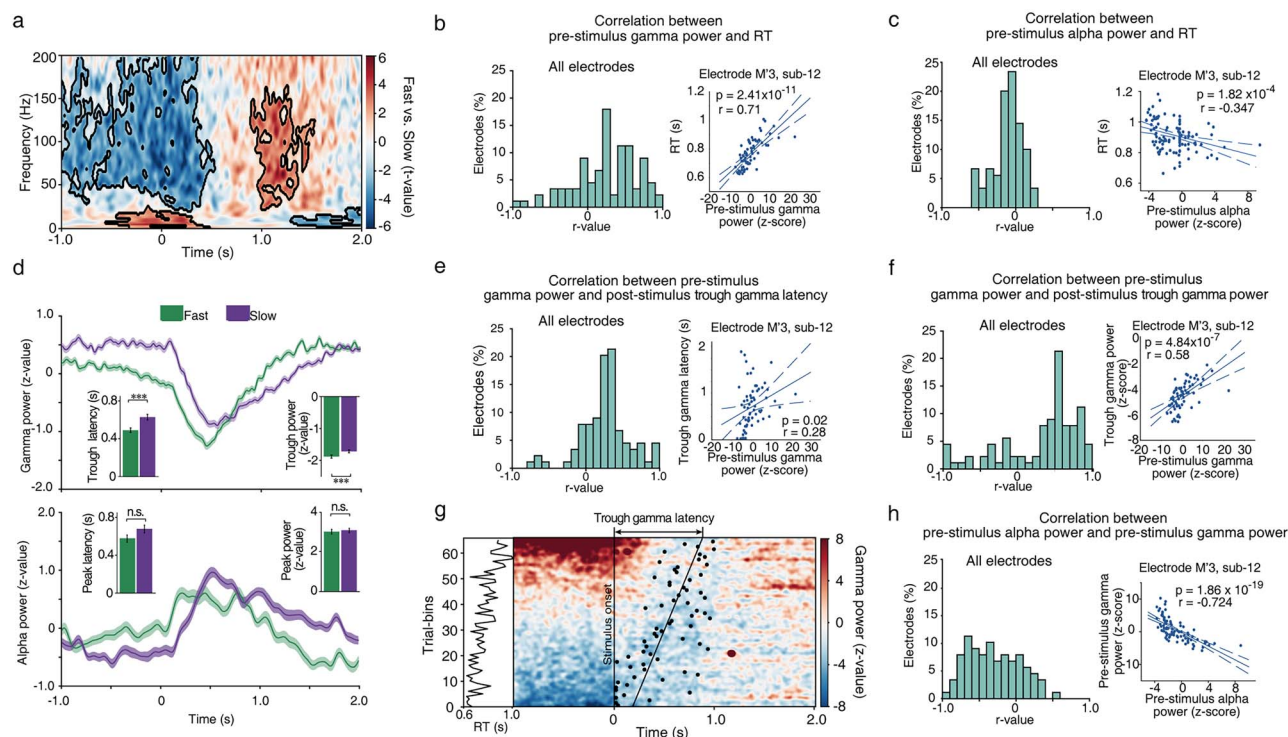


Fig. 2. Pre-stimulus gamma power in the DMN modulated behavior and task-induced DMN electrophysiological signatures in the auditory trials. (a) The time-frequency spectrum of t -values for the “fast > slow” comparison in the auditory trials. Time points zero marks the onset of the target stimulus. The significant clusters are outlined in black ($P < 0.05$, cluster-based permutation). The negative t -values (in blue) indicate lower gamma power in the fast than slow trials, whereas the positive t -values (in red) indicate higher gamma power in the fast than slow trials. (b) Distribution of all the responsive PMC electrode sites as a function of the correlation value between the pre-stimulus gamma power and the RTs. The correlation between the pre-stimulus gamma power and the RTs in a representative electrode is shown in the scatter figure. (c) The same as (b), except for the pre-stimulus alpha power. (d) The temporal profiles of the gamma (30–200 Hz, upper panel) and the alpha power (8–12 Hz, lower panel) are shown as a function of the fast vs. slow trials. Shaded error bars show within-subject standard error of the mean. The inserted bar graphs show the post-stimulus trough gamma latency and power, and the post-stimulus peak alpha latency and power in the fast vs. slow condition, respectively. Error bars represent the standard error of the mean. (e) Distribution of all the responsive PMC electrode sites as a function of with the correlation value between the pre-stimulus gamma power and the post-stimulus trough gamma latency. The scatter figure shows the correlation between the pre-stimulus gamma power and the post-stimulus trough gamma latency in the same representative electrode as in (b). (f) Distribution of all the responsive PMC electrode sites along the continuum of the correlation values between the pre-stimulus gamma power and the post-stimulus trough gamma power. The scatter figure shows the correlation between the pre-stimulus gamma power and the post-stimulus trough gamma power in the same representative electrode as in (b). (g) Surface plot of the gamma power spectrum in the trial-bins sorted by the pre-stimulus gamma power along the y -axis in the same representative electrode as in (b). The vertical line indicates the stimulus onset. The black dots represent the time points at which the post-stimulus gamma power reaches its maximum deactivation (i.e. latency) in each trial-bin, and the linear fit line is fitted for these time points. The left-most panel shows the mean RTs in each trial-bin. (h) Distribution of all the responsive PMC electrode sites along the continuum of the correlation values between the pre-stimulus gamma power and the pre-stimulus alpha power. The scatter figure shows the correlation between the pre-stimulus gamma power and the pre-stimulus alpha power in the same representative electrode as in (b). *** $P < 0.001$. RT, reaction time.

deactivation in the PMC. To demonstrate the modulatory effect of the pre-stimulus gamma power on the RTs and the latency of the post-stimulus maximal gamma deactivation, a surface plot was obtained from the same representative electrode (Fig. 2g). Each row represents the RT, the power and the latency of the maximal gamma suppression in each trial-bin, respectively, and the trial-bins were sorted by the pre-stimulus gamma power. It was clear that both the RTs and the latency of the post-stimulus maximal gamma deactivation increased gradually with the increasing pre-stimulus gamma power. As we identically z -transformed the time-frequency data in each and every auditory trial, rather than z -transformed the fast and the slow auditory trials, separately, the differences in power between the fast and the slow auditory trials should not be biased due to the z transformation.

To determine the relationship between the pre-stimulus gamma power and the pre-stimulus alpha power in the auditory trials, the LMMs were adopted as well. The results showed that the pre-stimulus gamma power was a significant predictor of the pre-stimulus alpha power, $\beta = -0.43$, $P < 2 \times 10^{-4}$. 72% of the

electrodes showed a negative correlation coefficient between the pre-stimulus gamma power and the pre-stimulus alpha power (Fig. 2h). Results from one representative electrode showed that the trials with higher pre-stimulus gamma power were associated with lower pre-stimulus alpha power (Fig. 2h, the scatter figure), suggesting anti-correlations between the pre-stimulus gamma and alpha power.

The same analyses were performed on the visual trials, and similar patterns of results were revealed (Fig. 3). The pre-stimulus gamma band power (30–200 Hz) was significantly lower in the fast than slow trials than in slow trials during pre-stimulus periods (Fig. 3a). LMM analyses showed that an increase in the pre-stimulus gamma power led to an increase in RTs, $\beta = 1.28$, $P = 7.43 \times 10^{-8}$, whereas an increase in the pre-stimulus alpha power led to a decrease in RTs, $\beta = -1.15$, $P = 0.05$. In addition, 74% of the electrodes showed a positive correlation coefficient between the pre-stimulus gamma power and the RTs (Fig. 3b), and 70% of the electrodes showed a negative correlation coefficient between the pre-stimulus alpha power and the RTs (Fig. 3c).

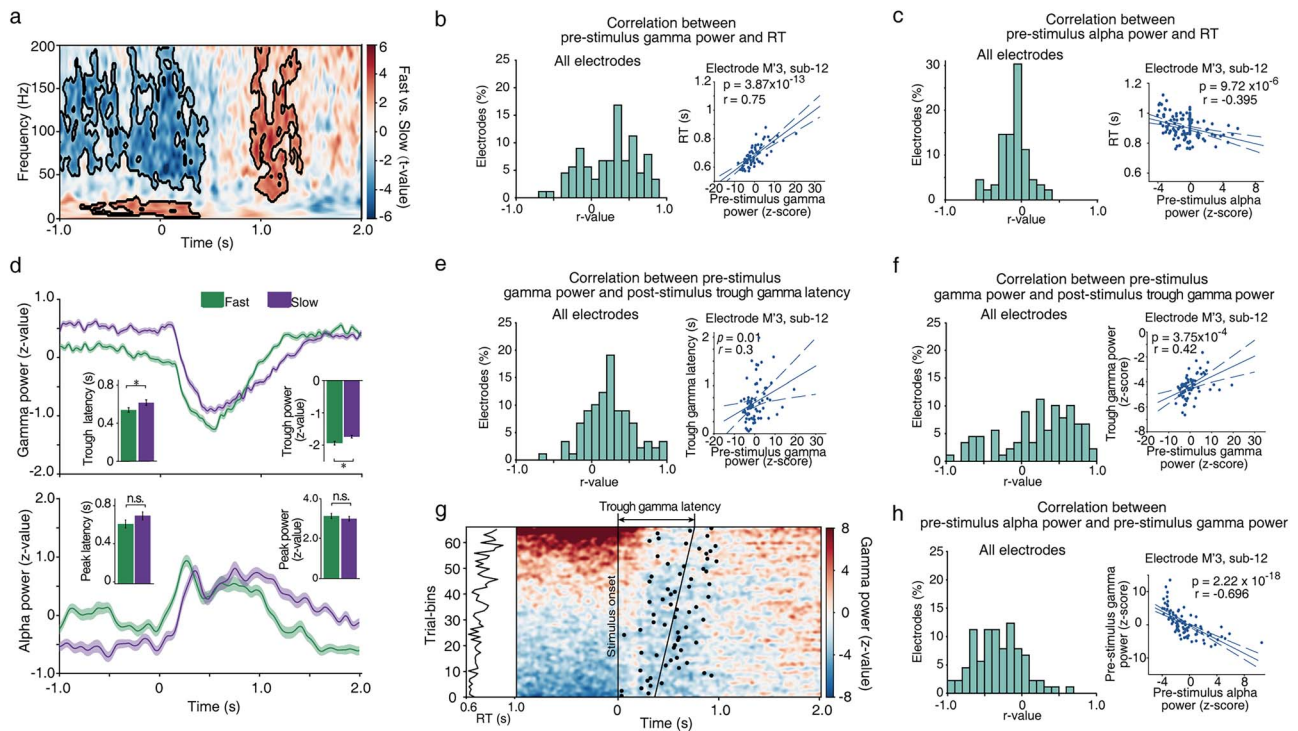


Fig. 3. Pre-stimulus gamma power in the DMN modulated behavior and task-induced DMN electrophysiological signatures in the visual trials. (a) The time-frequency spectrum of t -values for the “fast > slow” comparison in the auditory trials. Time points zero marks the onset of the target stimulus. The significant clusters are outlined in black ($P < 0.05$, cluster-based permutation). The negative t -values (in blue) indicate lower gamma power in the fast than slow trials, whereas the positive t -values (in red) indicate higher gamma power in the fast than slow trials. (b) Distribution of all the responsive PMC electrode sites as a function of the correlation value between the pre-stimulus gamma power and the RTs. The correlation between the pre-stimulus gamma power and the RTs in a representative electrode is shown in the scatter figure. (c) The same as (b), except for the pre-stimulus alpha power. (d) The temporal profiles of the gamma power (30–200 Hz, upper panel) and alpha power (8–12 Hz, lower panel) are shown as a function of the fast vs. slow trials. Shaded error bars show the within-subject standard error of the mean. The inserted bar graphs show the post-stimulus trough gamma latency and power, and the post-stimulus peak alpha latency and power in the fast vs. slow condition, respectively. Error bars represent the standard error of the mean. (e) Distribution of all the responsive PMC electrode sites as a function of the correlation values between the pre-stimulus gamma power and the post-stimulus trough gamma latency. The scatter figure shows the correlation between the pre-stimulus gamma power and the post-stimulus trough gamma latency in the same representative electrode as in (b). (f) Distribution of all the responsive PMC electrode sites along the continuum of correlation values between the pre-stimulus gamma power and the post-stimulus trough gamma power. The scatter figure shows the correlation between the pre-stimulus gamma power and the post-stimulus trough gamma power in the same representative electrode as in (b). (g) Surface plot of the gamma power spectrum in the trial-bins sorted by the pre-stimulus gamma power along the y -axis in the same representative electrode as in (b). The vertical line indicates the stimulus onset. The black dots represent the time points at which the post-stimulus gamma power reaches its maximum deactivation (i.e. latency) in each trial-bin, and the linear fit line is fitted for these time points. The left-most panel shows the mean RTs in each trial-bin. (h) Distribution of all the responsive PMC electrode sites along the continuum of the correlation values between the pre-stimulus gamma power and the pre-stimulus alpha power. The inset scatter figure shows the correlation between the pre-stimulus gamma power and the pre-stimulus alpha power in the same representative electrode as in (b). * $P < 0.05$. RT, reaction time.

For the post-stimulus period, the fast trials corresponded to a lower power (normalized amplitude in fast trials: -1.88 ± 0.06 ; in slow trials: -1.71 ± 0.04 , Fig. 3d upper panel, the right inserted bar figure), $t_{(88)} = -2.51$, $P = 0.01$, $d = -0.32$, and an earlier latency (fast trials: 547 ± 28 ms; slow trials: 618 ± 31 ms, Fig. 3d, upper panel, the left inserted bar figure), $t_{(88)} = -2.31$, $P = 0.02$, $d = -0.25$, of the maximal gamma suppression than the slow trials. LMM results confirmed these observations by showing that a lower pre-stimulus gamma power led to an earlier latency, $\beta = 4.81$, $P < 2 \times 10^{-16}$, and a lower power, $\beta = 0.05$, $P < 2 \times 10^{-16}$, of the task-induced maximal gamma deactivation in the PMC area. No such results were observed for the post-stimulus peak alpha latency, $t_{(88)} = -1.29$, $P = 0.20$, $d = -0.14$ (Fig. 3d, lower panel, the left inserted bar figure), and peak alpha power, $t_{(88)} = 1.71$, $P = 0.09$, $d = -0.12$ (Fig. 3d, lower panel, the right inserted bar figure).

Furthermore, the pre-stimulus gamma power showed a positive correlation coefficient with the post-stimulus trough gamma latency in 78% of the electrodes (Fig. 3e), and with the power of the task-induced maximal gamma deactivation in 74% of the

electrodes (Fig. 3f). Generally, both the RTs and the latency of the post-stimulus maximal gamma deactivation increased gradually with the increasing pre-stimulus gamma power (Fig. 3g). LMM results also showed that the pre-stimulus gamma power was a significant predictor of the pre-stimulus alpha power for the visual trials, $\beta = -0.40$, $P = 0.01$, and 76% of the electrodes showed a negative correlation coefficient between the pre-stimulus gamma power and the pre-stimulus alpha power (Fig. 3h). Taken together, the results in the visual trials showed a highly consistent pattern with the auditory trials.

Between-modality difference in the PMC

Subsequently, we aimed to explore the between-modality difference in the neural profile of the PMC. We first compared the time course of the gamma power between the visual (collapsed over all the visual trials) and the auditory (collapsed over all the auditory trials) modality. Results of the cluster-based permutation indicated that the gamma power in the visual trials was significantly lower than the auditory trials during the recovery

period from the maximal suppression to the baseline (Fig. 4a, right panel). However, there was no significant difference between the visual and the auditory trials, either in terms of the latency (visual trials: 520 ± 23 ms; auditory trials: 500 ± 27 ms), $t_{(88)} = 0.65$, $P = 0.52$, $d = 0.01$, or the power (normalized amplitude in visual trials: -2.23 ± 0.18 ; in auditory trials: -2.15 ± 0.16), $t_{(88)} = -1.16$, $P = 0.25$, $d = 0.07$, of the task-induced maximal gamma deactivation (Fig. 4a, bar figures in the right panel).

As individuals responded significantly faster to visual trials (686 ± 42 ms) than to auditory trials (703 ± 40 ms), $t_{(18)} = -2.06$, $P = 0.05$, $d = -0.01$ (Fig. 4a, left panel), it remains unknown whether the between-modality difference represents a modality-specific effect or an effect of task performance. Therefore, we further investigated this issue by dissociating the effect of task performance (RTs) at both the within-subject and the between-subject level.

Within-subject comparison

According to the behavioral results, the visual responses were generally faster than the auditory responses (Fig. 4a, left panel). For the fast trials, there was no significant RT difference between the fast visual trials (556 ± 30 ms) and the fast auditory trials (557 ± 33 ms), $t_{(18)} = -0.21$, $P = 0.83$, $d = -0.01$ (Fig. 4b, left panel). The between-modality difference in RTs, however, was mainly driven by the slow trials: the slow visual responses (814 ± 52 ms) were significantly faster than the slow auditory trials (850 ± 52 ms), $t_{(18)} = 3.12$, $P = 6.42 \times 10^{-3}$, $d = 0.16$ (Fig. 4c, left panel). Therefore, the between-modality difference in the gamma temporal profile (Fig. 4a, right panel) could be caused either by the difference in response speed or by the different sensory modalities per se. We hypothesized that if the between-modality difference is driven by the different sensory modalities per se, it should still exist when the between-modality difference in RTs was eliminated in the fast trials. To test this hypothesis, we compared the gamma time course between the visual and the auditory trials in the fast and the slow trials, respectively.

For the fast trials, the gamma power of the auditory trials was still significantly higher than the visual trials during the recovery period from the maximal suppression to the baseline (Fig. 4b, right panel), $P = 0.001$, cluster-based permutation. No significant between-modality difference was found either for the latency (visual trials: 520 ± 23 ms; auditory trials: 500 ± 27 ms), $t_{(88)} = 0.65$, $P = 0.52$, $d = 0.01$, or the power (normalized amplitude in visual trials: -3.23 ± 0.18 ; in auditory trials: -3.15 ± 0.16), $t_{(88)} = -1.00$, $P = 0.32$, $d = -0.05$, of the task-induced maximal gamma deactivation (Fig. 4b, bar figures in the right panel). For the slow trials, however, there was no significant difference between the visual and the auditory trials in temporal profile of gamma (Fig. 4c, right panel). Also, no significant between-modality difference was found either for the latency (visual trials: 649 ± 30 ms; auditory trials: 700 ± 33 ms), $t_{(88)} = -1.64$, $P = 0.11$, $d = -0.17$, or for the amplitude (normalized amplitude in visual trials: -3.01 ± 0.14 ; in auditory trials: -2.89 ± 0.16), $t_{(88)} = -1.3$, $P = 0.20$, $d = -0.07$, of the post-stimulus maximal gamma deactivation (Fig. 4c, bar figures in the right panel).

Between-subject comparison

The within-subject comparisons between the visual and auditory trials, as a function of the fast and the slow trials, showed that the higher gamma power in the auditory than visual trials during the recovery period from the maximal suppression to the baseline represents a clean between-modality difference, rather than a response speed effect. However, as the clean between-modality difference was confined to the fast trials, one may

argue that this effect only applies to the situations when the brain is in a high-efficiency status. To further confirm and generalize this conclusion across all the trials, we performed between-subject comparisons by categorizing the subjects into two groups (see Methods). In the response matched group, the visual (765 ± 95 ms) and the auditory (746 ± 114 ms) response speed (collapsed over all the trials in one modality within a subject) was comparable, $t_{(7)} = 0.56$, $P = 0.59$, $d = 0.07$ (Fig. 5a, left panel), whereas in the response unmatched group, the visual responses (676 ± 55 ms) were significantly faster than the auditory responses (773 ± 62 ms), $t_{(10)} = -2.92$, $P = 0.02$, $d = -0.36$ (Fig. 5b, left panel).

At the neural level, for the response matched group, there was a significant difference in the gamma power between the auditory and visual trials during the gamma recovery period, $P = 0.001$, cluster-based permutation (Fig. 5a, right panel). However, there was no significant difference between the visual and the auditory modality, either in terms of the latency (visual trials: 585 ± 28 ms; auditory trials: 563 ± 36 ms), $t_{(41)} = 0.66$, $P = 0.51$, $d = 0.11$, or the power (normalized amplitude in visual trials: -3.43 ± 0.19 ; in auditory trials: -3.29 ± 0.19), $t_{(41)} = -1.25$, $P = 0.22$, $d = -0.12$, of the post-stimulus maximal gamma deactivation (Fig. 5a, bar figures in the right panel). For the response unmatched group, there was no significant between-modality difference in the gamma neural profile (Fig. 5b, right panel). Also, no significant between-modality difference was found either for the latency (visual trials: 535 ± 33 ms; auditory trials: 510 ± 30 ms), $t_{(46)} = 0.81$, $P = 0.48$, $d = 0.12$, or the power (normalized amplitude in visual trials: -2.21 ± 0.19 ; in auditory trials: -2.14 ± 0.16), $t_{(46)} = -0.94$, $P = 0.35$, $d = -0.06$, of the post-stimulus maximal gamma deactivation (Fig. 5b, bar figures in the right panel). To further rule out the possibility that the between-modality difference in the gamma temporal profiles was only specific to the 20-ms cutoff we chose to categorize the matched and unmatched subject group, we further calculated the between-modality difference in the matched vs. unmatched group at another two cutoffs (10 and 30 ms). The new results at the 10- and 30-ms cutoffs showed high consistency with the results at the 20-ms cutoff (see Supplementary Fig. 4).

To summarize, the within- (Fig. 4b and c) and between-subject (Fig. 5) comparisons together suggested that with the task performance being comparable between the visual and the auditory modality, the auditory responses in the PMC recovered faster from the maximal suppression to the baseline than the visual responses.

Discussion

Upon repetitively performing the same well-practiced behavioral task on the same bottom-up sensory inputs, our task performance still varies dramatically. It has been well documented that elevated pre-stimulus baseline activity in the DMN impairs the subsequent task performance (Weissman et al. 2006; Boly et al. 2007; Hayden et al. 2009; Kucyi et al. 2020). It remains unknown, however, how variation in the pre-stimulus baseline activity of the DMN impacts the temporal dynamics of the task-induced DMN deactivation. In the present study, we clearly demonstrated that the elevated pre-stimulus baseline activity of the DMN resulted in three consequences: (i) the DMN was less deactivated during the task performance; (ii) it took a longer time for the DMN deactivation to reach its maximal suppression; and (iii) it took longer for the task-induced DMN deactivation to return back to the baseline (Figs. 2 and 3).

It has been well documented that the gamma power of the DMN significantly decreases, relative to the pre-stimulus baseline,

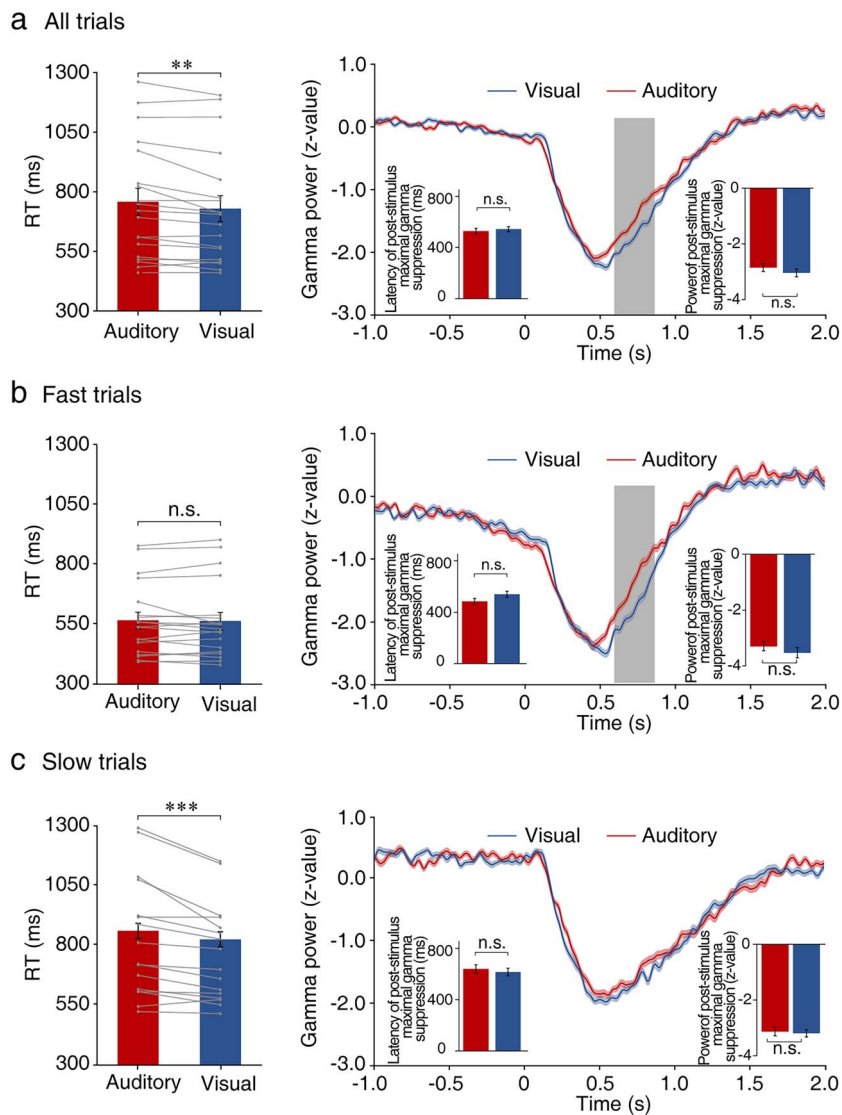


Fig. 4. Modality-specific mechanisms in DMN—within-subject comparisons. (a) Direct comparison between the visual and auditory modalities, collapsed over all the trials in each modality. The left panel: the mean RTs in the visual and auditory modalities. The light gray lines depict the mean RTs of each subject in the visual and auditory trials. The right panel: temporal dynamics of the gamma power in the DMN are shown as a function of the visual vs. auditory modality. Shaded regions around each waveform denote ± 1 within-subjects standard error of the mean. The inserted bar figures show the latency and the power of the post-stimulus maximal gamma suppression in the visual and auditory trials. The error bars represent the standard error of the mean. (b) Comparisons between the visual and auditory processing in the fast trials. (c) Comparison between the visual and auditory processing in the slow trials. The time windows marked by the gray bars showed statistically significant difference between the visual and auditory trials, at $P < 0.05$, corrected for multiple comparisons using the cluster-based permutation test. ** $P < 0.01$, *** $P < 0.001$. RT, reaction time.

during a variety of demanding cognitive tasks, such as visual search (Ossandón et al. 2011), reading (Lachaux et al. 2008; Jerbi et al. 2010), backward-masking visual categorization (Ramot et al. 2012), arithmetic calculation (Dastjerdi et al. 2011; Foster et al. 2012, 2015), etc. Moreover, the more complex the cognitive tasks, the longer the RTs, and the stronger the task-induced gamma suppression in the DMN (Ossandón et al. 2011). Also, compared with behavioral errors, correct responses correspond to a stronger task-induced gamma power deactivation as well (Kucyi et al. 2020). The longer RTs in the more complex cognitive tasks and the correct responses both indicate that the brain enters a more efficient task state when higher levels of executive control are involved, compared with the easier tasks or behavioral errors. In the present experimental setup, however, the longer RTs represent a less efficient, whereas the faster RTs represent a more efficient task state of the brain. Specifically speaking, upon performing

the same behavioral task on the same bottom-up inputs, the slower RTs simply indicate worse task performance, whereas the faster RTs simply indicate better task performance. Therefore, consistent with the stronger gamma suppression in the DMN during the complex (slower RTs) than easy (faster RTs) task (Ossandón et al. 2011), the faster RT trials in the present study were associated with stronger gamma suppression in the DMN than the slower RT trials (Fig. 2a and 3a). In addition, the stronger gamma suppression in the fast trials also reached its maximal suppression faster (i.e. a shorter latency), and returned to the baseline faster, compared with the slow trials (Figs. 2d and 3d, upper panel).

Please note, the differential post-stimulus DMN dynamics between the complex vs. easy task were induced by the different task demands (Ossandón et al. 2011). However, the differential post-stimulus DMN dynamics between the fast vs. slow responses

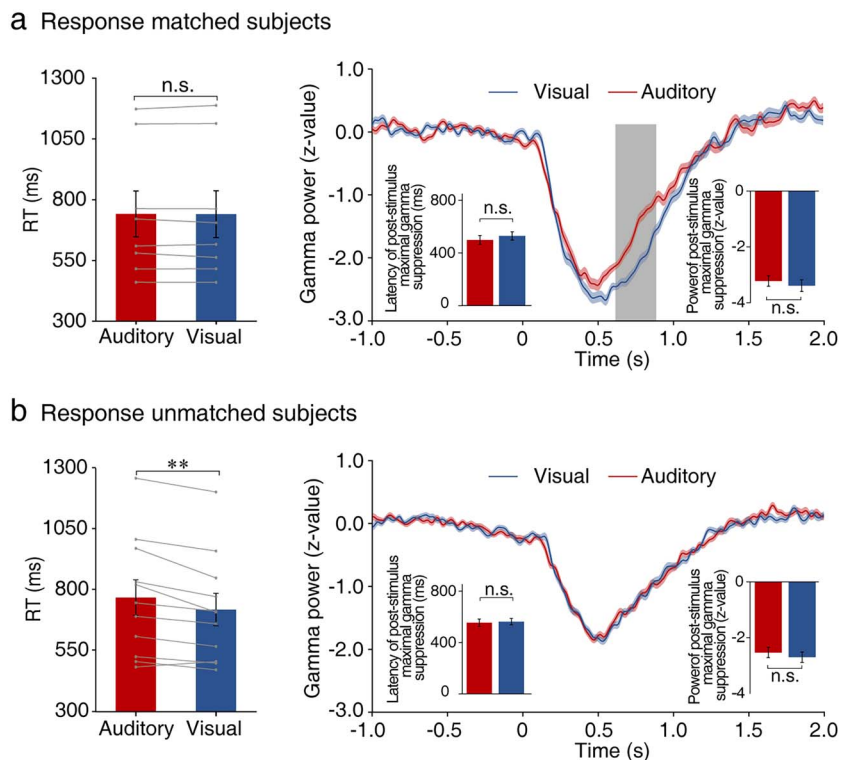


Fig. 5. Modality-specific mechanism in DMN—between-subject comparisons. (a) Comparison between the visual and auditory trials in the subjects who responded to the visual and auditory targets comparably fast. The left panel: the RTs of the visual and auditory trials. The light gray lines depict the mean RTs of each subject in the visual and auditory trials. The right panel: the temporal dynamics of the gamma power in the DMN are shown as a function of the visual vs. auditory modality. Shaded regions around each waveform denote ± 1 within-subjects standard error of the mean. The inserted bar figures show the latency (ms) and the power (z-value) of the post-stimulus maximal gamma suppression during the visual and auditory processing. Error bars represent the standard error of the mean. (b) Comparison between the visual and auditory trials in the subjects whose auditory RTs were significantly slower than visual RTs. The time windows marked by the gray bars showed statistically significant difference between the visual and auditory trials, at $P < 0.05$, corrected for multiple comparisons using the cluster-based permutation test. $**P < 0.01$, $***P < 0.001$. RT, reaction time.

in the present study were pre-determined by the pre-stimulus baseline activity in the DMN (Figs. 2 and 3). It has been well documented that the spontaneous fluctuations of neural activity in the DMN prior to a behavioral task result in different task outcomes: the more elevated the pre-stimulus DMN activity, the worse the behavioral performance in stimulus-driven and attention-demanding tasks (Eichele et al. 2008; Esterman et al. 2013; Li et al. 2007; Sali et al. 2016; Soravia et al. 2016; Weissman et al. 2006; Su et al. 2020). Functionally, the elevated pre-stimulus DMN activity has been associated with momentary lapses of attention and task-irrelevant mind-wandering (Logothetis et al. 2001; Weissman et al. 2006; Vincent et al. 2007; Parvizi and Kastner 2018). In the present study, we further showed how the elevated pre-stimulus DMN activity led to worse task performance. Specifically, the pre-activated DMN makes it less efficient not only to transit from the pre-stimulus baseline to the task-induced suppression, in terms of a lower task-induced maximal suppression and a longer latency, but also less efficient to recover from the maximal suppression to the baseline activity (Figs. 2d and 3d, upper panel).

Previous evidence showed that the more complex the behavioral task, the longer the RTs, and the slower the recovery time from the task-induced DMN maximal suppression to the baseline activity (Ossandón et al. 2011). In the present study, we also found that the task-induced DMN maximal suppression returned to the baseline significantly slower in the longer than shorter RT trials (Figs. 2d and 3d, upper panel). Note, the longer RTs in the previous

complex task and the longer RTs in the present study have different functional implications: a higher level of executive control and efficiency of the brain in the former case vs. simply a lower efficiency state of the brain in the latter case. Therefore, a slower recovery from the maximal suppression to the baseline in both cases indicates a generally slower motor response. Furthermore, our results showed that the mean latency of the task-induced maximal gamma deactivation in the DMN was 179 ms earlier than the mean RT, which positioned the response period well in the recovery phase from the maximal suppression to the baseline. Therefore, together with previous evidence, the present results implied that the amplitude and the latency of the task-induced maximal suppression in the DMN may index the efficiency of earlier sensory and central executive functions. For example, both the longer RTs in the previous complex tasks (Ossandón et al. 2011) and the shorter RTs in the present study represent a high efficiency state of the human brain, and are accordingly both associated with deeper and faster task-induced maximal suppression in the DMN. On the other hand, the speed of the later recovery from the maximal suppression to the baseline may index the speed of motor responses. For example, both the longer RTs in the previous complex task (Ossandón et al. 2011) and the longer RTs in the present study are associated with a slower recovery speed from the maximal suppression to the baseline in the DMN.

It has been suggested that the gamma oscillation in the visual cortex plays an important role in visual perception by facilitating

the forward-transfer of information through the cortical hierarchy (Bosman et al. 2012; Jia et al. 2013; Roberts et al. 2013; for reviews, see Sedley and Cunningham 2013) and/or inhibiting the activity of task-irrelevant regions (Tadin et al. 2003; Gieselmann and Thiele 2008; Chalk et al. 2010; for reviews see Sedley and Cunningham 2013). Accordingly, the higher gamma power in the visual cortex, the better the individuals' performance (Osipova et al. 2006; Womelsdorf et al. 2006; Edden et al. 2009; Fisch et al. 2009). In contrast to the visual gamma, the lower pre-stimulus alpha power in visual areas is predictive of better task performance both in humans and non-human primates (Ergenoglu et al. 2004; Thut et al. 2006; Hanslmayr et al. 2007; van Dijk et al. 2008; Zhang et al. 2008). Moreover, it has been revealed, in V1 of awake macaques, that the alpha power is anti-correlated with the gamma power (Spaak et al. 2012). In the present study, we found similar anti-correlations between the pre-stimulus gamma and alpha power in human PMC (Figs. 2h and 3h). However, the functional roles of the PMC gamma and alpha power were inverse to those of the visual gamma and alpha. Specifically speaking, a positive correlation between the pre-stimulus PMC gamma power and the RTs (Figs. 2b and 3b), and a negative correlation between the pre-stimulus PMC alpha power and RTs (Figs. 2c and 3c) were revealed in the present study. The lower pre-stimulus gamma power and the higher pre-stimulus alpha power led to better task performance, i.e. shorter RTs. Together with previous evidence, the present results suggested a general anti-correlation between the gamma and the alpha power across the PMC and the visual cortex while inverse functional roles of the PMC vs. the visual cortex on task performance, along both the gamma and the alpha bands. Visual effects can be induced by electrical stimulation of the PMC boundary electrode sites close to the visual cortex (Foster and Parvizi 2017). However, when the boundary stimulations were excluded, no positive visual effects were observed within the PMC, indicating that the PMC visual effects might be caused by the interference of the visual cortex, rather than a real function of the PMC. Therefore, the underlying functions of the PMC are fundamentally different from the visual cortex. The present results implied that the DMN needs to be sufficiently suppressed, in terms of low gamma and high alpha power, in order for the task-related cortex (e.g. visual cortex) to maintain high processing efficiency, in terms of high gamma and low alpha power. To verify this speculation, future studies will need to investigate how the between-regional coherence in the gamma and alpha band between the DMN and the sensory cortex affects task performance.

In addition, via direct comparisons between the visual and the auditory trials, we investigated the between-modality difference in the DMN neural profile. The photo-transduction in the retina is slower than the process of sound transduction by the hair cells of the inner ear (Corey and Hudspeth 1979; Schnapf et al. 1987), and the neural transmission time from the sense organs to the cerebral cortex is longer in the visual system due to the greater distances involved (Fain 2003; King 2005b). Accordingly, the detection time of visual stimuli is longer than the detection time of auditory stimuli (Dunlap and Wells 1910; Jose and Gideon Praveen 2010). However, the auditory processing advantages could be eliminated in multisensory environments when both visual and auditory stimuli could appear (Koppen and Spence 2007; Huang et al. 2015; Yue et al. 2015). Behavioral data in the present multisensory paradigm further showed that the mean auditory detection times became even slower than the mean visual detection times (Fig. 4a). At the neural level, when the visual and the auditory stimuli induced identical DMN deactivation

neural profiles, the visual responses were significantly faster than the auditory responses (Figs. 4c and 5b). To match the response speed between the two modalities, the visual responses need to be relatively slowed down, whereas the auditory responses need to be speeded up. Accordingly, in the match conditions (Figs. 4b and 5a), we observed a longer recovery time from the maximal suppression to the baseline in the DMN during the visual than auditory trials, with the amplitude and the latency of the maximal suppression being comparable between the two modalities. Evidence from previous fMRI studies showed that the BOLD responses in human PMC were significantly more deactivated during visual than auditory perception when the visual and auditory response speed was comparable (Daselaar et al. 2010; Huijbers et al. 2011). The present results further suggested that the more deactivated PMC gamma power during visual than auditory processing happened during the recovery period from the maximal suppression back to the baseline activity, approximately 650–950 ms after the stimulus onset (Fig. 4a, right panel). The average visual and auditory RTs in the present study were both around 700 ms (visual trials: 686 ms, auditory trials: 703 ms) (Fig. 4a, left panel), which positioned the manual responses well within the recovery period in PMC. These neural and behavioral results together implied that the efficiency of earlier sensory processing might be comparable between the visual and the auditory modalities, whereas the between-modality difference might happen during the later response period.

To summarize, via high temporal resolution intracranial recording, we revealed the precise temporal dynamics underlying how variation in the pre-stimulus baseline activity of the DMN translates to the subsequent varying task performance when the human brain operates the same behavioral task on the same bottom-up inputs. For the first time in the field, we showed that elevated pre-stimulus gamma power in the DMN alleviates the task-induced suppression, delays its latency to reach the maximal suppression, and slows down its return to the baseline, which eventually results in deleterious effects on task performance. The above neural dynamics in the DMN occur, irrespectively of the input sensory modality. As we adopted simple detection tasks in the present study, it remains to be further investigated whether similar DMN neural dynamics apply to more complex tasks.

Funding

National Natural Science Foundation of China (31871138, 32071052, 32000741, 32000785), the Natural Science Foundation of Guangdong Province (2021A1515011100, 2020A1515110223, 2021A1515011185), the Guangzhou Fundamental Research Program (202102020761, 202102020274) and the MOE Project of Key Research Institute of Humanities and Social Sciences in Universities (22JJD190006).

Notes

The authors wish to thank all of subjects who volunteered their time, without whom this project would not have been possible.

Conflict of interest statement: None declared.

Data and code availability statement

All the data and code are available at <https://osf.io/khsyf/>. The data and code used in the study are available in the public domain for its sharing or re-use. The data and code sharing adopted by the

authors comply with the requirements of the institute and comply with institutional ethics approval.

References

- Baayen RH, Davidson DJ, Bates DM. Mixed-effects modeling with crossed random effects for subjects and items. *J Mem Lang*. 2008;59:390–412.
- Bates D, Mächler M, Bolker BM, Walker SC. Fitting linear mixed-effects models using lme4. *J Stat Softw*. 2015;67:1–48.
- Boly M, Balteau E, Schnakers C, Degueldre C, Moonen G, Luxen A, Phillips C, Peigneux P, Maquet P, Laureys S. Baseline brain activity fluctuations predict somatosensory perception in humans. *Proc Natl Acad Sci U S A*. 2007;104:12187–12192.
- Bosman CA, Schoffelen JM, Brunet N, Oostenveld R, Bastos AM, Womelsdorf T, Rubehn B, Stieglitz T, De Weerd P, Fries P. Attentional stimulus selection through selective synchronization between monkey visual areas. *Neuron*. 2012;75:875–888.
- Chalk M, Herrero JL, Gieselmann MA, Delicato LS, Gotthardt S, Thiele A. Attention reduces stimulus-driven gamma frequency oscillations and spike field coherence in V1. *Neuron*. 2010;66:114–125.
- Corey DP, Hudspeth AJ. Response latency of vertebrate hair cells. *Biophys J*. 1979;26:499–506.
- Daselaar SM, Porat Y, Huijbers W, Pennartz CMA. Modality-specific and modality-independent components of the human imagery system. *NeuroImage*. 2010;52:677–685.
- Dastjerdi M, Foster BL, Nasrullah S, Rauschecker AM, Dougherty RF, Townsend JD, Chang C, Greicius MD, Menon V, Kennedy DP, et al. Differential electrophysiological response during rest, self-referential, and non-self-referential tasks in human posteromedial cortex. *Proc Natl Acad Sci U S A*. 2011;108:3023–3028.
- Desikan RS, Ségonne F, Fischl B, Quinn BT, Dickerson BC, Blacker D, Buckner RL, Dale AM, Maguire RP, Hyman BT. An automated labeling system for subdividing the human cerebral cortex on MRI scans into gyral based regions of interest. *NeuroImage*. 2006;31:968–980.
- Dunlap K, Wells GR. Some experiments with reactions to visual and auditory stimuli. *Psychol Rev*. 1910;17:319.
- Edden RAE, Muthukumaraswamy SD, Freeman TCA, Singh KD. Orientation discrimination performance is predicted by GABA concentration and gamma oscillation frequency in human primary visual cortex. *J Neurosci*. 2009;29:15721–15726.
- Eichele T, Debener S, Calhoun VD, Specht K, Engel AK, Hugdahl K, Von Cramon DY, Ullsperger M. Prediction of human errors by maladaptive changes in event-related brain networks. *Proc Natl Acad Sci*. 2008;105:6173–6178.
- Ergenoglu T, Demiralp T, Bayraktaroglu Z, Ergen M, Beydagi H, Uresin Y. Alpha rhythm of the EEG modulates visual detection performance in humans. *Cogn Brain Res*. 2004;20:376–383.
- Esterman M, Noonan SK, Rosenberg M, DeGutis J. In the zone or zoning out? Tracking behavioral and neural fluctuations during sustained attention. *Cereb Cortex*. 2013;23:2712–2723.
- Fain GL. *Sensory transduction*. Sunderland, MA: Sinauer Associates; 2003.
- Fischl L, Privman E, Ramot M, Harel M, Nir Y, Kipervasser S, Andelman F, Neufeld MY, Kramer U, Fried I, et al. Neural “ignition”: enhanced activation linked to perceptual awareness in human ventral stream visual cortex. *Neuron*. 2009;64:562–574.
- Fischl B, Salat DH, Busa E, Albert M, Dieterich M, Haselgrove C, Van Der Kouwe A, Killiany R, Kennedy D, Klaveness S, et al. Whole brain segmentation: automated labeling of neuroanatomical structures in the human brain. *Neuron*. 2002;33:341–355.
- Foster BL, Parvizi J. Direct cortical stimulation of human posteromedial cortex. *Neurology*. 2017;88:685–691.
- Foster BL, Dastjerdi M, Parvizi J. Neural populations in human posteromedial cortex display opposing responses during memory and numerical processing. *Proc Natl Acad Sci U S A*. 2012;109:15514–15519.
- Foster BL, Rangarajan V, Shirer WR, Parvizi J. Intrinsic and task-dependent coupling of neuronal population activity in human parietal cortex. *Neuron*. 2015;86:578–590.
- Fox KCR, Foster BL, Kucyi A, Daitch AL, Parvizi J. Intracranial electrophysiology of the human default network. *Trends Cogn Sci*. 2018;22:307–324.
- Gieselmann MA, Thiele A. Comparison of spatial integration and surround suppression characteristics in spiking activity and the local field potential in macaque V1. *Eur J Neurosci*. 2008;28:447–459.
- Groppe DM, Bickel S, Dykstra AR, Wang X, Mégevand P, Mercier MR, Lado FA, Mehta AD, Honey CJ. iELVis: an open source MATLAB toolbox for localizing and visualizing human intracranial electrode data. *J Neurosci Methods*. 2017;281:40–48.
- Hanslmayr S, Aslan A, Staudigl T, Klimesch W, Herrmann CS, Bäuml KH. Prestimulus oscillations predict visual perception performance between and within subjects. *NeuroImage*. 2007;37:1465–1473.
- Hayden BY, Smith DV, Platt ML. Electrophysiological correlates of default-mode processing in macaque posterior cingulate cortex. *Proc Natl Acad Sci U S A*. 2009;106:5948–5953.
- Huang S, Li Y, Zhang W, Zhang B, Liu X, Mo L, Chen Q. Multisensory competition is modulated by sensory pathway interactions with fronto-sensorimotor and default-mode network regions. *J Neurosci*. 2015;35:9064–9077.
- Huijbers W, Pennartz CMA, Rubin DC, Daselaar SM. Imagery and retrieval of auditory and visual information: neural correlates of successful and unsuccessful performance. *Neuropsychologia*. 2011;49:1730–1740.
- Humphreys GF, Hoffman P, Visser M, Binney RJ, Lambon Ralph MA. Establishing task- and modality-dependent dissociations between the semantic and default mode networks. *Proc Natl Acad Sci U S A*. 2015;112:7857–7862.
- Jerbi K, Vidal JR, Ossandon T, Dalal SS, Jung J, Hoffmann D, Minotti L, Bertrand O, Kahane P, Lachaux JP. Exploring the electrophysiological correlates of the default-mode network with intracerebral EEG. *Front Syst Neurosci*. 2010;4:1–9.
- Jia X, Tanabe S, Kohn A. Gamma and the coordination of spiking activity in early visual cortex. *Neuron*. 2013;77:762–774.
- Jose S, Gideon Praveen K. Comparison between auditory and visual simple reaction times. *Neurosci Med*. 2010;2010:30–32.
- Jung J, Jerbi K, Ossandon T, Ryvlin P, Isnard J, Bertrand O, Guénot M, Mauguière F, Lachaux JP. Brain responses to success and failure: direct recordings from human cerebral cortex. *Hum Brain Mapp*. 2010;31:1217–1232.
- Kamp T, Sorger B, Benjamins C, Hausfeld L, Goebel R. The prestimulus default mode network state predicts cognitive task performance levels on a mental rotation task. *Brain Behav*. 2018;8:1–10.
- Kemp HG Jr, Vokonas PS, Cohn PF, Gorlin R. The anginal syndrome associated with normal coronary arteriograms: report of a six year experience. *Am J Med*. 1973;54:735–742.
- King AJ. Multisensory integration: strategies for synchronization. *Curr Biol*. 2005a;15:R339–R341.
- King AJ. Multisensory Intergration: strategies for synchronization. *Curr Biol*. 2005b;15:339–341.
- Koppen C, Spence C. Spatial coincidence modulates the Colavita visual dominance effect. *Neurosci Lett*. 2007;417:107–111.
- Kriegeskorte N, Simmons WK, Bellgowan PS, Baker CI. Circular analysis in systems neuroscience: the dangers of double dipping. *Nat Neurosci*. 2009;12:535–540.

- Kriegeskorte N, Lindquist MA, Nichols TE, Poldrack RA, Vul E. Everything you never wanted to know about circular analysis, but were afraid to ask. *J Cereb Blood Flow Metab.* 2010;30:1551–1557.
- Kucyi A, Daitch A, Raccah O, Zhao B, Zhang C, Esterman M, Zeinhe M, Halpern CH, Zhang K, Zhang J, et al. Electrophysiological dynamics of antagonistic brain networks reflect attentional fluctuations. *Nat Commun.* 2020;11:1–14.
- Kuznetsova A, Brockhoff PB, Christensen RHB. lmerTest package: tests in linear mixed effects models. *J Stat Softw.* 2017;82:1–26.
- Lachaux JP, Jung J, Mainy N, Dreher JC, Bertrand O, Baciou M, Minotti L, Hoffmann D, Kahane P. Silence is golden: transient neural deactivation in the prefrontal cortex during attentive reading. *Cereb Cortex.* 2008;18:443–450.
- Li C-SR, Yan P, Bergquist KL, Sinha R. Greater activation of the “default” brain regions predicts stop signal errors. *NeuroImage.* 2007;38:640–648.
- Logothetis NK, Pauls J, Augath M, Trinath T, Oeltermann A. Neurophysiological investigation of the basis of the fMRI signal. *Nature.* 2001;412:150–157.
- Maris E, Oostenveld R. Nonparametric statistical testing of EEG- and MEG-data. *J Neurosci Methods.* 2007;164:177–190.
- Marshall WH, Talbot SA. Recent evidence for neural mechanisms in vision leading to a general theory of sensory acuity. In: Klüver H., (ed). *Biological Symposia-Visual mechanisms.* Lancaster, PA: Cattell. 1942:117–164.
- McKiernan KA, Kaufman JN, Kucera-Thompson J, Binder JR. A parametric manipulation of factors affecting task-induced deactivation in functional neuroimaging. *J Cogn Neurosci.* 2003;15:394–408.
- Miller KJ, Leuthardt EC, Schalk G, Rao RPN, Anderson NR, Moran DW, Miller JW, Ojemann JG. Spectral changes in cortical surface potentials during motor movement. *J Neurosci.* 2007;27:2424–2432.
- Miller KJ, Weaver KE, Ojemann JG. Direct electrophysiological measurement of human default network areas. *Proc Natl Acad Sci U S A.* 2009;106:12174–12177.
- Narizzano M, Arnulfo G, Ricci S, Toselli B, Tisdall M, Canessa A, Fato MM, Cardinale F. SEEG assistant: a 3DSlicer extension to support epilepsy surgery. *BMC Bioinformatics.* 2017;18:1–13.
- Oostenveld R, Fries P, Maris E, Schoffelen JM. FieldTrip: open source software for advanced analysis of MEG, EEG, and invasive electrophysiological data. *Comput Intell Neurosci.* 2011;2011:156869.
- Osipova D, Takashima A, Oostenveld R, Fernández G, Maris E, Jensen O. Theta and gamma oscillations predict encoding and retrieval of declarative memory. *J Neurosci.* 2006;26:7523–7531.
- Ossandón T, Jerbi K, Vidal JR, Bayle DJ, Henaff M, Jung J, Minotti L, Bertrand O, Kahane P, Lachaux J. Transient suppression of broadband gamma power in the default-mode network is correlated with task complexity. *J Neurosci.* 2011;31:14521–14530.
- Parvizi J, Kastner S. Promises and limitations of human intracranial electroencephalography. *Nat Neurosci.* 2018;21:474–483.
- Raichle ME, Gusnard DA. Intrinsic brain activity sets the stage for expression of motivated behavior. *J Comp Neurol.* 2005;493:167–176.
- Raichle ME, MacLeod AM, Snyder AZ, Powers WJ, Gusnard DA, Shulman GL. A default mode of brain function. *Proc Natl Acad Sci U S A.* 2001;98:676–682.
- Ramot M, Fisch L, Harel M, Kipervasser S, Andelman F, Neufeld MY, Kramer U, Fried I, Malach R. A widely distributed spectral signature of task-negative electrocorticography responses revealed during a visuomotor task in the human cortex. *J Neurosci.* 2012;32:10458–10469.
- Roberts MJ, Lowet E, Brunet NM, TerWal M, Tiesinga P, Fries P, DeWeerd P. Robust gamma coherence between macaque V1 and V2 by dynamic frequency matching. *Neuron.* 2013;78:523–536.
- Sali AW, Courtney SM, Yantis S. Spontaneous fluctuations in the flexible control of covert attention. *J Neurosci.* 2016;36:445–454.
- Schnapf JL, Kraft TW, Baylor DA. Spectral sensitivity of human cone photoreceptors. *Nature.* 1987;325:439–441.
- Sedley W, Cunningham MO. Do cortical gamma oscillations promote or suppress perception? An under-asked question with an over-assumed answer. *Front Hum Neurosci.* 2013;7:1–17.
- Shulman GL, Corbetta M, Buckner RL, Fiez JA, Miezin FM, Raichle ME, Petersen SE. Common blood flow changes across visual tasks., I. increases in subcortical structures and cerebellum but not in nonvisual cortex. *J Cogn Neurosci.* 1997;9:648–663.
- Soravia LM, Witmer JS, Schwab S, Nakataki M, Dierks T, Wiest R, Henke K, Federspiel A, Jann K. Prestimulus default mode activity influences depth of processing and recognition in an emotional memory task. *Hum Brain Mapp.* 2016;37:924–932.
- Spaak E, Bonnefond M, Maier A, Leopold DA, Jensen O. Layer-specific entrainment of gamma-band neural activity by the alpha rhythm in monkey visual cortex. *Curr Biol.* 2012;22:2313–2318.
- Su W, Guo Q, Li Y, Zhang K, Zhang Y, Chen Q.. Momentary lapses of attention in multisensory environment. *Cortex.* 2020;131:195–209.
- Tadin D, Lappin JS, Gilroy LA, Blake R. Perceptual consequences of centre-surround antagonism in visual motion processing. *Nature.* 2003;424:312–315.
- Thut G, Nietzel A, Brandt SA, Pascual-Leone A. α -Band electroencephalographic activity over occipital cortex indexes visuospatial attention bias and predicts visual target detection. *J Neurosci.* 2006;26:9494–9502.
- van Dijk H, Schoffelen J-M, Oostenveld R, Jensen O. Prestimulus oscillatory activity in the alpha band predicts visual discrimination ability. *J Neurosci.* 2008;28:1816–1823.
- Vincent JL, Patel GH, Fox MD, Snyder AZ, Baker JT, Van Essen DC, Zempel JM, Snyder LH, Corbetta M, Raichle ME. Intrinsic functional architecture in the anaesthetized monkey brain. *Nature.* 2007;447:83–86.
- Weissman DH, Roberts KC, Visscher KM, Woldorff MG. The neural bases of momentary lapses in attention. *Nat Neurosci.* 2006;9:971–978.
- Womelsdorf T, Fries P, Mitra PP, Desimone R. Gamma-band synchronization in visual cortex predicts speed of change detection. *Nature.* 2006;439:733–736.
- Yue Z, Jiang Y, Li Y, Wang P, Chen Q. Enhanced visual dominance in far space. *Exp Brain Res.* 2015;233:2833–2843.
- Zhang Y, Wang X, Bressler SL, Chen Y, Ding M. Prestimulus cortical activity is correlated with speed of visuomotor processing. *J Cogn Neurosci.* 2008;20:1915–1925.
- Zhang M, Wang X, Goldberg ME. A spatially nonselective baseline signal in parietal cortex reflects the probability of a monkey’s success on the current trial. *Proc Natl Acad Sci U S A.* 2014;111:8967–8972.